Automated Embryo Manipulation and Rotation via Robotic nDEP-Tweezers

Kaicheng Huang, Ihab Abu Ajamieh, Zhenxi Cui, Jiewen Lai, James K. Mills, *Member, IEEE*, and Henry K. Chu, *Member, IEEE*

***Abstract*—Embryo manipulation is a fundamental task in assisted reproductive technology (ART). Nevertheless, conventional pick-place techniques often require proper alignment to avoid causing damage to the embryo and further, the tools have limited capability to orient the embryo being handled. *Objective:* This paper presents a novel and non-invasive technique that can easily manipulate mouse embryos on a polyvinyl chloride (PVC) Petri dish. *Methods:* An inverted microchip with quadrupole electrodes was attached to a micromanipulator to become a robotic dielectrophoresis (DEP) tweezers, and a motorized platform provided additional mobility to the embryos lying on a Petri dish. Vision-based algorithms were developed to evaluate relevant information of the embryos from the image, and to provide feedback signals for precise position and orientation control of the embryo. *Results:* A series of experiments was conducted to examine the system performance, and the embryo can be successfully manipulated to a specified location with the desired orientation for subsequent processing. *Conclusion:* This system offers a non-contact, low cost, and flexible method for rapid cell handling. *Significance:* As the DEP tweezers can grasp the embryo without the need for precise alignment, the overall time required to process a large number of embryos can be shortened.**

***Index Terms*—Control, embryo manipulation, micro manipulation, negative dielectrophoresis, visual servo.**

I. Introduction

ASSISTED reproductive technology refers to the procedures of manipulating eggs, sperms, and embryos to treat infertility. Common treatments used to fertilize embryos include in vitro fertilization (IVF) [1] and intracytoplasmic sperm injection (ICSI) [2]. In addition, embryos can be treated to facilitate in vitro embryo production and development, such as assisted zona hatching, preimplantation genetic diagnosis (PGD), cloning, gene expression analysis, and cell replacement therapy (CRT). Although all these techniques have helped thousands of infertile couples, many of them need to be performed by fully trained operators, with the training process which could take more than a year. Besides, the success rate of embryo manipulation and transfer is relatively low. Knowing that the membrane of an embryo is very fragile, improper handling can cause damage to the embryo [3]. Therefore, having a reliable method to interact with the embryo is necessary.

In the last decades, robotic systems have emerged to replace and automate the manual manipulation of cells and embryos. Applying the image process technique for cell classification and recognition [4], these systems have been successfully applied to various biomedical applications, such as embryo manipulation [5]–[7], cell injection [8], ICSI [9], embryo biopsy [10] and assisted hatching [11]. However, all these systems employ a contact-based method to interact with the cell. In the contact-based method, the adhesion force between the cell and the tool cannot be ignored because the surface area in contact is comparable to the overall size of a cell. To overcome the adhesion force in micro-scale manipulation, Chu *et al.* [12] employed a dual-arm micromanipulation system to release a micro-scale object through the coordinated motion from two probe tips. Coating or surface treatment can also be applied to modify the surface properties to reduce the adhesion force. However, there is a possibility that the cells could escape from the tool during manipulation. Holding cells inside a pipette is another option to avoid direct contact between the tool and the cell. Liu *et al.* [13] developed a robotic verification system with a micropipette that can pick and place a single embryo at a time. The micropipette was held in position by a micromanipulator and a syringe pump was used to suck the embryo inside the pipette during translation. Zhang *et al.* [14] further enhanced the system by enabling multiple embryo translation for verification. A bubble actuated system has benn developed for indirectly contacted micromanipulation [15] and the system can be also applied to the cell manipulation [16]. No matter which contact-based method is used, precise alignment or positioning of the tool with respect to the cell is still required, which could consume a significant amount of time. Therefore, different non-contact methods for cell handling have also been studied.

The mechanism to manipulate cells without any direct contact can generally be categorized as magnetic force [17], hydrodynamic force [18], optical force [19], electrophoresis [20], and dielectrophoresis [21]. For instance, Eguchi *et al.* [22] demonstrated to change the orientation of rat Schwann cells

Manuscript received July 11, 2020; revised August 26, 2020; accepted October 3, 2020. Date of publication October 14, 2020; date of current version June 18, 2021. The work was supported by the Research Grant Council of the Hong Kong Special Administrative Region, China, under Grant 25204016. *(Corresponding author: Henry K. Chu)*

Kaicheng Huang, Zhenxi Cui, and Jiewen Lai are with the Department of Mechanical Engineering, The Hong Kong Polytechnic University.

Ihab Abu Ajamieh and James K. Mills are with the Department of Mechanical and Industrial Engineering, University of Toronto.

Henry K. Chu is with the Department of Mechanical Engineering, The Hong Kong Polytechnic University, Hong Kong (e-mail: henry.chu@polyu.edu.hk).

Digital Object Identifier 10.1109/TBME.2020.3031043

using a magnetic field, with the field providing weak alignment for proteins. Collin *et al.* [23] used acoustic waves for high-throughput patterning of polystyrene (PS) beads into individual microwell. However, the use of hydrodynamic force is more effective to control cells in batch rather than individually. Li *et al.* [24] used a feedback control system to achieve high precision single-cell translation with an optical tweezers. Orientation control can also be achieved through an optical tweezers by Bayoudh *et al.* [25]. Xie *et al.* [26] used a robot-aided optical tweezers manipulation system to achieve automated translation and rotation control for a biological cell. However, one limitation of the optical tweezers is that the particle size needs to be 100um or smaller. Yang *et al.* [27] utilized a parallel trapping and optical releasing mechanism that can selectively remove any trapped particles with an optical beam. Jiang *et al.* [28] used a quadrupole electrode to achieve cell rotation with DEP. Park *et al.* [29] employed both hydrodynamic and DEP forces to achieve embryo translation and orientation. Since the effective region by DEP is limited, cell translation over a long distance remains a challenging task. Besides, similar to the magnetic force manipulation, using a strong electric field to improve the efficiency is not recommended as it could pose a threat to the biological cells.

In recent years, the advancements in Lab-on-a-Chip (LOC) and microfluidic devices have enabled efficient biological cell assay and analysis at the cellular level [18]. A number of LOC devices have been designed for use with embryos. For example, Glasgow *et al.* [30] built a microfluidic device for mammalian embryo translation. Choi *et al.* [31] used the electric field to sort healthy oocytes flowing through the microchannel for IVF. Valley *et al.* [32] employed light-induced DEP to assess the response of embryos. Park *et al.* [29] integrated a valve into a microfluidic device to rotate immobilized embryos. Raty *et al.* [33] enhanced the culture environment through microchannel for embryonic development. While all these assays are successfully carried out in a sealed environment, there is limited accessibility from outside of the chip. Also, it is difficult to transfer the embryos out of the chip for subsequent culture and analysis.

In this study, we aim to offer a flexible solution to facilitate screening, sorting, and characterizing embryos lying on a glass slide or Petri dish. In contrast to contact-based methods, this proposed method does not require high precision when handling the embryos. The limitation of short traveling distance in the non-contact method can be overcome through the integration of a robotic manipulation system. In our previous study, a quadrupole electrodes microchip was first designed to study yeast cell rotation via electrorotation (ER) [28]. We had also developed a micromanipulation system that can provide 3-D positioning between a microchip and a substrate for cell patterning [34]. The effects of different experimental parameters on the patterning efficiency were studied in [35]. In this study, we combined the quadrupole electrode microchip and the micromanipulation system for rapid embryo manipulation. Control algorithms based on visual images were developed so that the embryo can be manipulated to the specified location with the desired orientation. A series of tests was performed to validate the effectiveness and robustness of the system.

II. Principle of DEP and ER

This work employs DEP to manipulate embryos in the medium and the working principle is to utilize electrode pairs to generate non-uniform electric fields in the aqueous environment. As described by Pohl [37], any dielectric particle exposed to an alternating electric field can be polarized and a DEP force is induced on the particle. Here, we review the relevant theory of DEP, from [37]. The DEP force, F_{DEP}, acting on two sides of the particle can be evaluated as:

$$F_{DEP} = 2\pi r^3 \varepsilon_m \cdot Re[K(\omega)] \cdot \bigtriangledown E^2 \tag{1}$$

where r is the particle radius, ε_m is the permittivity of the suspending medium, $\bigtriangledown$ is the Del vector operator, and E is the root mean square of the electric field. $Re[K(\omega)]$ is the real part of the Clausius–Mossotti (CM) factor. The CM factor represents the interaction between the particle and the medium which can be evaluated as:

$$K(\omega) = \frac{\varepsilon_p^* - \varepsilon_m^*}{\varepsilon_p^* + 2\varepsilon_m^*} \tag{2}$$

where ε^* is the complex permittivity of the particle and suspension medium, as represented by subscripts p and m, respectively. Complex permittivity can be written as:

$$\varepsilon^* = \varepsilon - j\frac{\sigma}{\omega} \tag{3}$$

where $j = \sqrt{-1}$, σ is the conductivity, and ε is the permittivity. ω is the angular frequency of applied voltage. By selecting different frequencies of the input signal, the sign of real or imaginary part of the CM factor can be changed so as to reverse the direction of the DEP force and ER torque.

Similar to the DEP phenomenon, the working principle of ER is to use the electric field to change the orientation of a particle in a circular movement. A rotating or alternating electric field should be applied to a set of electrodes surrounding the cell to induce ER for cell rotation. The rotation torque acting on the cell can be given by [38]:

$$\tau_{ER} = -4\pi r^3 \varepsilon_m \cdot Im[K(\omega)] \cdot |E|^2 \tag{4}$$

where ε_m is the permittivity of the suspension medium. r is the radius of the particle. $Im[K(\omega)]$ is the imaginary part of the CM factor. $|E|$ is the strength of the electric field.

As the particle in the aqueous environment experiences a hydrodynamic force, a rotating particle is subjected to a hydrodynamic torque T_f, which can be represented as:

$$T_f = 8\pi\eta\Omega r^3 \tag{5}$$

where η is the viscosity of the medium.

To evaluate the resultant angular speed $\Omega(\omega)$ on a particle which experiences the ER, it can be obtained by combining (4) and (5), which is given by:

$$\Omega(\omega) = -\frac{\varepsilon_m Im[K(\omega)]|E|^2}{2\eta} \tag{6}$$

This equation indicates that Ω is correlated to the strength and the frequency of the electric field, with the properties of the medium and the particle are known.

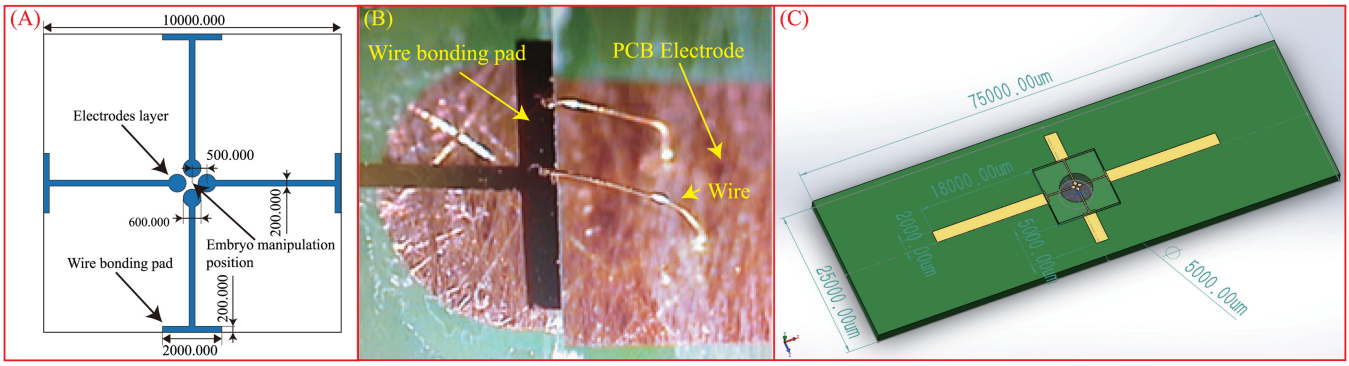

Fig. 1. Illustration of the microchip.

TABLE I
PROPERTIES OF EMBRYO [36]

	Blastomere	Zona pellucida
Conductivity $\sigma(S/m)$	50	$\frac{19.1\times10^{-6}}{400\times10^{-4}}$
Relative permittivity ε	$70\varepsilon_0$	$19.1\times10^{-6} * 1.25\times10^{-2}$
Radius $r(\mu m)$	36	55.1

The electrical properties of a biological cell have been studied by a number of groups [39], [40] and a cell can be modeled as a multi-shell particle. For an oocyte, it can be modeled as a two-layer sphere with a polar body and zona pellucida [36], and its electrical properties through measurements are listed in Table I. Huang *et al.* [41] proposed a general formula to represent the multi-shell particle as a homogeneous particle and determine their electrical properties through a smeared-out approach. The inner (layer 1) and the adjacent layer (layer 2) are remodeled as a homogeneous particle. Equivalent electrical properties can be evaluated and progressed layer-by-layer toward the outermost layer (layer N). The equivalent complex permittivity of the first two layers can be represented as:

$$\varepsilon^*_{1,e} = S(\varepsilon^*_1, \varepsilon^*_2, R_1, R_2) = \varepsilon^*_2\left[\left(\frac{R_2}{R_1}\right)^3 + 2(\varepsilon^*_1 - \varepsilon^*_2) /(\varepsilon^*_1 + 2\varepsilon^*_2)/\left[\left(\frac{R_2}{R_1}\right)^3 + 2(\varepsilon^*_1 - \varepsilon^*_2)/(\varepsilon^*_1 + 2\varepsilon^*_2)\right]\right] \quad (7)$$

where ε^* and R are the complex permittivity and the radius of the first two layers, respectively.

During the embryo development, the DEP response behaves in a different manner from the 1-cell-to-Morula stage to the blastocyst stage [32], owing to the morphology difference. For a mouse embryo in the 1-cell-to-Morula stage, it can be treated as a two shell-layer sphere similar to the oocyte.

III. System Setup

A. Microchip Design for Embryo Trapping and Rotation

The microchip consists of four circular electrodes to create a zone (manipulation area) for transferring the embryo, as well as for embryo rotation. Negative-dielectrophoresis (nDEP) was considered so as to repel the embryo toward the center of the zone, minimizing the joule heating effect on the embryo from the electrode surfaces. The distance between the center of the cavity to the center of individual electrodes was set to 500 μm to provide sufficient space to surround the embryo, whereas the radius of the individual electrodes was 300 μm, leaving a 200 μm$\times$200 μm area for cell manipulation (Fig. 1A). The microchip, with a size of 10 mm $\times$ 10 mm, was mounted to a 75 mm $\times$ 25 mm printed circuit board (PCB) for wire connection, as shown in Fig. 1B. A 500 μm-diameter hole was cut in the PCB board so that the transparent microchip can be observed through the microscope (Fig. 1C).

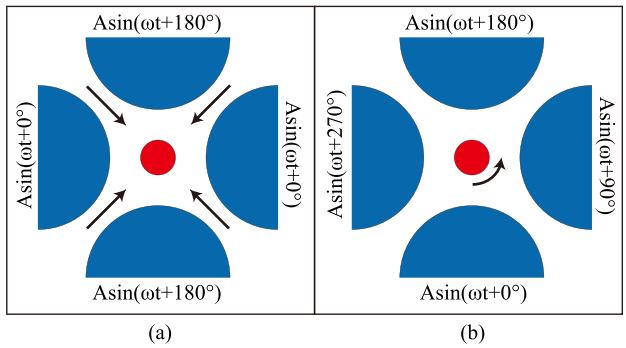

Fig. 2. Input signal for energizing electrode (a). Input signal for embryo translation (b). Input signal for embryo orientation.

Two two-channel function generators were used to provide voltages to the quadrupole electrodes for embryo orientation and translation, as shown in Fig. 2. Different sinusoidal signals were set to each of the electrodes. For embryo translation, the four electrodes were split into two pairs. Two electrodes that are opposite to each other were formed as the first pair and supplied voltage with the same phase, whereas the other electrode-pair was supplied voltage with the out-of-phase (Fig. 2A), leading to the generation of a non-uniform electric field (Fig. 3A). For embryo rotation, a rotating electric field was generated in the microenvironment (Fig. 3B). Four synchronized sinusoidal signals with a 90° phase difference were supplied to each of the electrode (Fig. 2B).

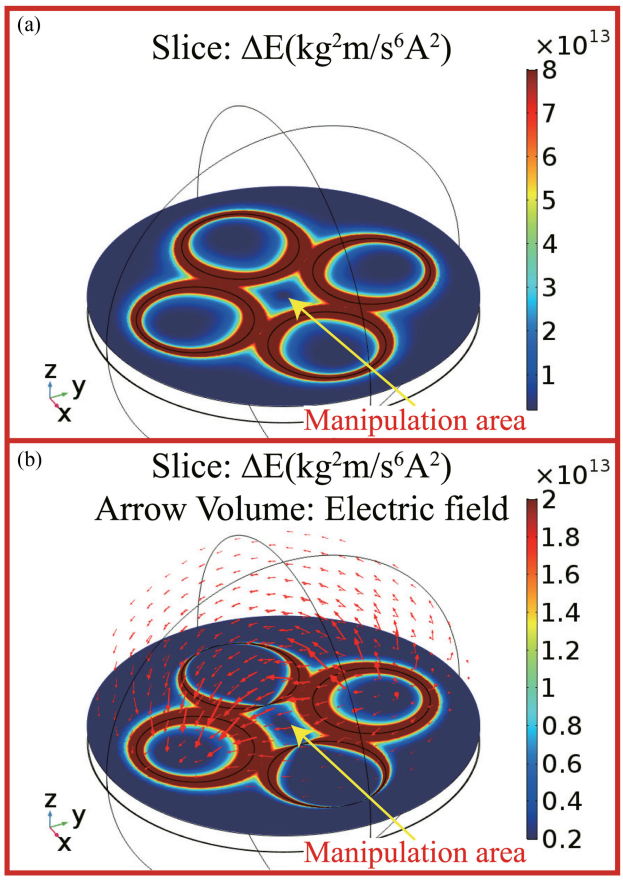

Fig. 3. (a). Static electric field simulation of quadrupole design (b). Rotation electric field simulation of quadrupole design.

Multiphysics software COMSOL was used to simulate the result for analysis. The quadrupole electrodes were modeled as four circular disks, whereas the medium was modeled as a sphere with a radius of 500 μm. The input signals were set according to Fig. 2A to obtain a closed electric field for embryo translation. The cross-section (slice) in Fig. 3A shows the strength of electric field gradient at the surface of the microchip. The high electric field gradient area is represented by the regions in red, which is located around the edge of the electrodes, forming a closed region with a low electric field gradient at the center of the microchip, represented by the blue color. The simulation of ER was also performed. With the input signals from Fig. 2B, a rotating electric field would be generated. The simulation result is shown in Fig. 3B where the arrow volume in the simulation shows the direction of the electric field which is related to the phenomenon of ER.

B. Design of the Micromanipulation System

For a conventional microfluidic device, a PDMS cover is used to form an irreversible microchannel that allows the target cell to flow through the electrodes on a substrate. For each new application, it is necessary to design the electrodes as well as the cover according to the needs. Also, there is a cost associated with the fabrication. Aiming to improve the flexibility and reusability, a micromanipulation system was proposed in our previous study [34] to create an adjustable 3D environment between the substrate and the microchip. In this study, a similar structure was set up and the Petri dish with embryos was placed on the motorized stage of the inverted microscope to provide planar movement. The microchip was inverted and mounted a 3D micromanipulator (Scientifica) (as shown in Fig. 4), to provide accurate positioning with respect to the Petri dish. The microchip was properly calibrated during the setup so that the microchip surface is aligned and parallel to the substrate. The microchip was connected to two synchronized function generators and the signal outputs were programmed via API through a computer. A control interface was developed, which can display images from the microscope to facilitate coordinated movements between the micromanipulator, the motorized platform, and the signal outputs. The entire system was placed on an anti-vibration table to minimize perturbations during experiments. The complete setup of the embryo manipulation system is shown in Figs. 4C and D.

C. Preparation of Cell Media and Substrate

Mouse embryos at their early stage were selected to examine non-contact manipulation via nDEP. These embryos were obtained by means approved by the University of Toronto Health Sciences Research Ethics Board (HSREB) and the Local Animal Care Committee (LACC). All embryos were first resuspended in standard DMEM medium. Since the adhesion between the embryos and the substrate material is dependent on the material properties of the substrate, a hydrophobic material could help to minimize the effect [35]. In this regard, a PVC Petri dish was selected over the glass Petri dish, and lower strength electric field can be used to reduce the invasiveness to the embryos.

IV. Methods

A top-view illustrating the procedure for aligning and orienting multiple embryos is shown in Fig. 5. First, to grasp an embryo with the quadrupole electrodes, the motorized stage of the microscope is manipulated to bring the target embryo to the center of the quadrupole electrodes (Fig. 5A). The electrodes are then energized to hold the embryo at the center of the quadrupole electrodes by DEP force (Fig. 5B). The stage is then manipulated and the trapped embryo is transferred to align with the next embryo following the planned path along with the x and y directions as shown in Figs. 5C–5D. After alignment, ER can be performed to rotate each embryo to the desired orientation (Figs. 5E–5F). In order to better illustrate the change in the orientation, paired PS beads were used for demonstration. Three pairs of PS beads were aligned and rotated as shown in Figs. 5G–5I.

A. Embryo Recognition

In order to facilitate embryo manipulation based on visual images, an object detection algorithm was developed to evaluate the relative position of the embryo within the region of interest. Given that the embryo also must be rotated, the orientation

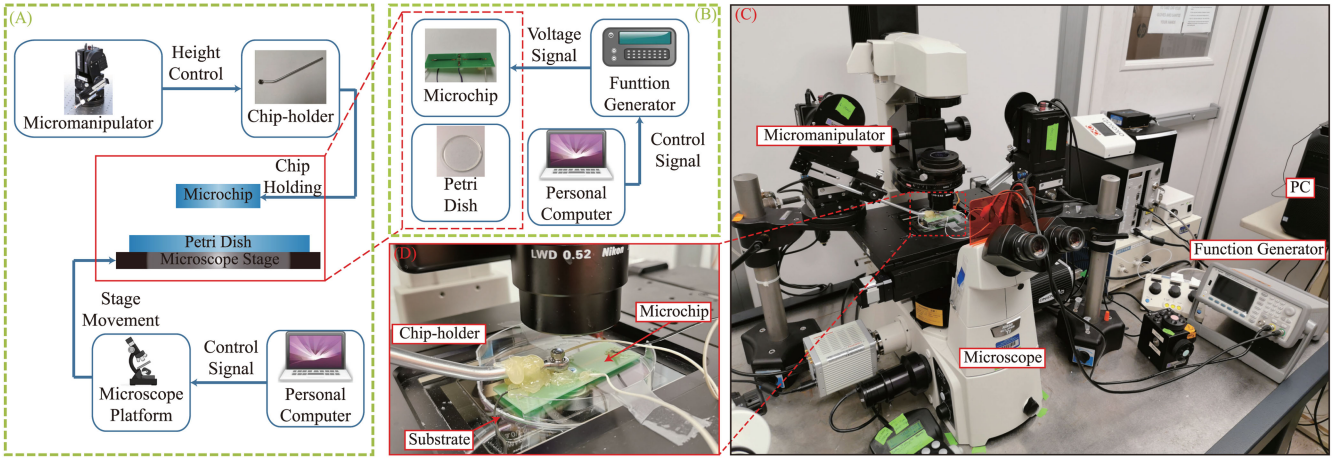

Fig. 4. (A,B). The diagram of the system setup (A). Components of system mechanical setup (B). Components for cell manipulation parts (C,D). Real image (c). Real image of experimental setup (D). The zoomed view of the working area.

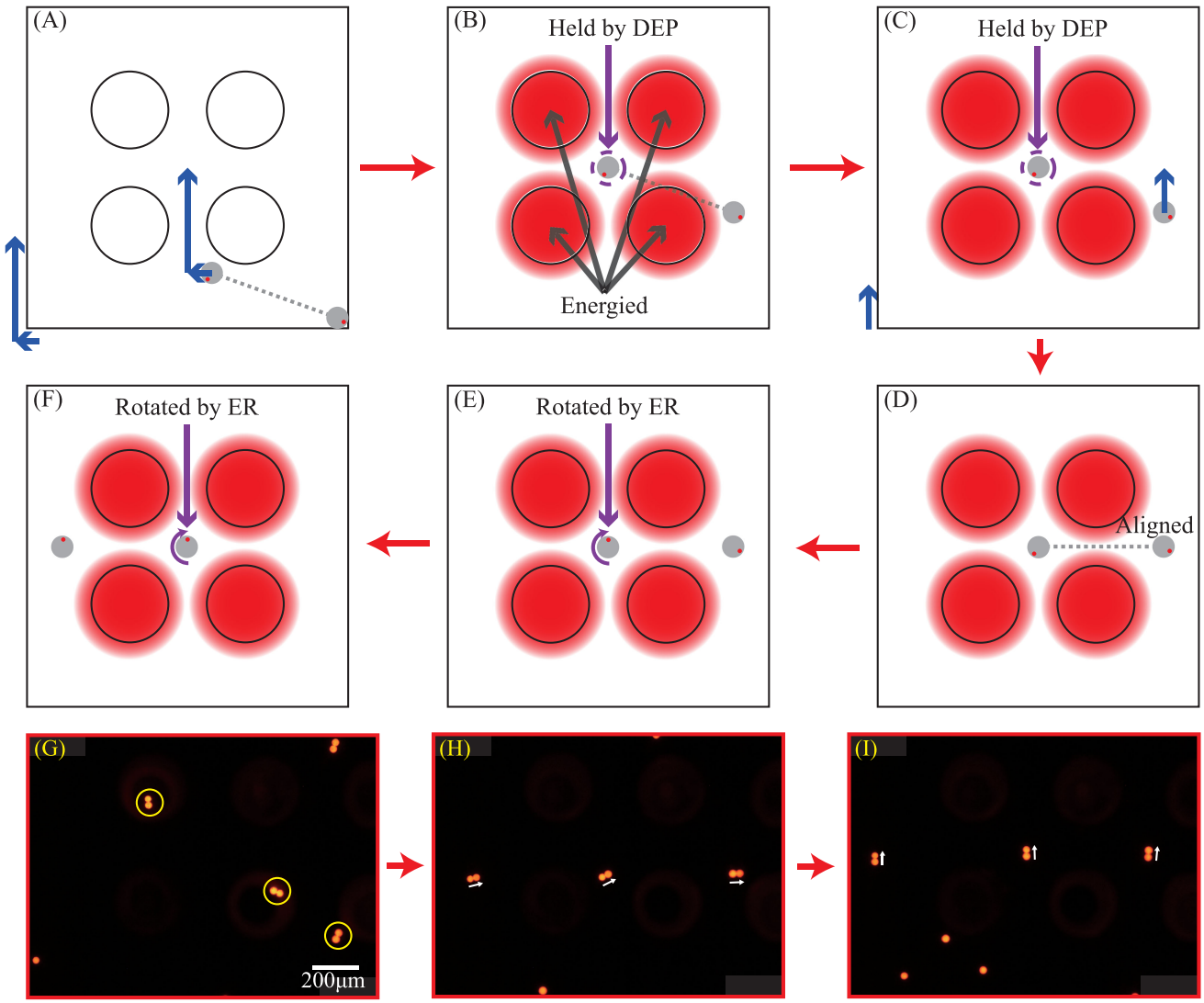

Fig. 5. The procedure of embryo alignment and rotation (A). Move the target embryo to the center of quadrupole electrode (B). Energize the quadrupole electrodes with the function generator and the embryo is held by DEP force (C). Move another embryo upward (D). The embryos are aligned horizontally (E). Rotate one of the embryo upward (F). Rotate another embryo upward (G). Three pairs of PS beads (H). The PS beads pairs are horizontal aligned (H). The three pairs of horizontal aligned PS beads are rotated to the same direction.

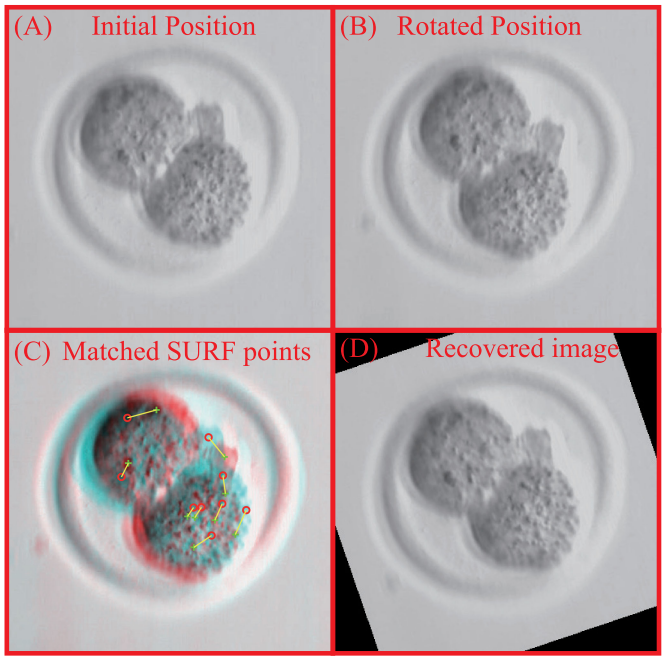

Fig. 6. Images with match function (A). Image of embryo in initial position (B). Image of embryo after rotated with certain angle (C). Matched points with SURF (D). Recovered image with the output information.

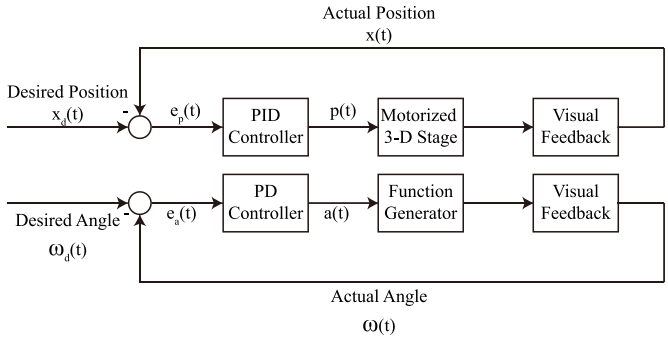

Fig. 7. Control scheme for embryo translation and rotation.

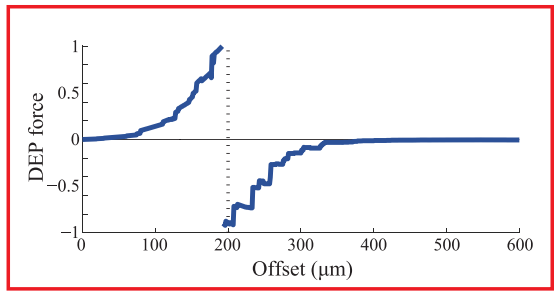

Fig. 8. Simulation of normalized DEP force versus position.

information of the embryo will be evaluated as well. Details of the detection algorithms are summarized below.

After an image was acquired with API, a Gaussian filter was applied to smoothen the image. A morphological filter was then applied to remove the background noise so that a clear image of the embryo can be observed. The position of the embryo can be obtained by finding the centroids of the connected region.

In this work, the embryos were in the one-cell stage. Since the zona pellucida and the blastomere are relatively round in shape, a feature-based approach was employed to acquire the orientation of the embryo. A MATLAB function "estimateGeometricTransform" was used to estimate the rotation difference between the adjacent pictures in the video streaming. By detecting and comparing the SURF feature [42] between two adjacent pictures, the geometric transformation, including the translation and the orientation, can be obtained (Fig. 6). By defining the initial orientation as 0°, the relative angular position (rotation angle) can be obtained.

To evaluate the viability of the embryo, the morphological evaluation was employed to monitor the zona pellucida and the blastomere. At present, morphological evaluation using microscopy remains the most apparent way to assess the viability of an embryo [43], while fluorescent staining had also been considered in other studies [44].

B. Embryo Translation With PID Control

A PID controller was used to precisely control the position of the trapped embryo in order to closely follow the planned path.

The PID controller is given as:

$$p(t) = K_p e_p(t) + K_i \int_0^t e_p(\tau)\, d\tau + K_d \frac{de_p(t)}{dt} \tag{8}$$

where $e_p(t) = x_d(t) - x(t)$ is the position error between the desired embryo position $x_d(t)$ along the path and the actual embryo position $x(t)$. A region of interest was drawn to obtain the actual position of the embryo in the next step $x(t+1)$. Given that the motorized stage was used to provide the relative motion between the trapped embryo and the substrate, $p(t)$ is the required input to the motorized stage for embryo translation. A schematic of the control system for embryo translation is shown in Fig. 7.

DEP force was primarily used to hold the embryo against the motion from the substrate. Fig. 8 shows the simulation of normalized DEP force acting on the embryo and the force has an asymptotic discontinuity at the boundary of the electrode ($x_o = 200\mu m$), in which the direction of the force changes in the opposite direction and is similar to the optical tweezers [45]. Therefore, an analogous controller was proposed to constrain the stage displacement so that the embryo can stay within the effective region for trapping. The input for the stage is given as:

$$u(t_o) \begin{cases} p(t_o), & |p| < x_o \quad (9a) \\ x_o, & p \geq x_o \quad (9b) \\ -x_o, & -p \leq -x_o \quad (9c) \end{cases}$$

C. Embryo Rotation With PID Control

Similar to the PID control for embryo translation, the PID controller for embryo rotation is given as:

$$a(t) = K_p e_a(t) + K_i \int_0^t e_a(\tau)\, d\tau + K_p \frac{de_a(t)}{dt} \tag{10}$$

where $e_a(t) = \omega_d(t) - \omega(t)$ is the angular position error between the desired embryo orientation angle $\omega_d(t)$ and the actual embryo angle $\omega(t)$.

As the rotation torque is directly proportional to the strength of the electric field as shown in (4), changing the voltage of the input signal can also modify the rotation torque. Therefore, the input of the controller a(t) is set as the voltage of the input signal. The control scheme for embryo rotation is shown in Fig. 7.

V. Results

A series of experiments was conducted to examine the performance of the proposed system for embryo translation and rotation. First, the effect of the microchip height was explored to obtain the proper manipulation input voltage. The embryo was also tested to move to the desired location while moving the stage at various speeds. The use of the PID controller to transport an embryo to the desired location through the DEP-tweezers was examined. Next, the embryo was rotated with open-loop control, with different voltage and frequency inputs applied to validate embryo rotation by ER. The optimal parameters used in the PID controller were also evaluated experimentally. Finally, the controller was implemented to the system and the embryo was arbitrarily rotated to different angular positions.

A. Effect of the Microchip Height From Embryo

Although an electric field can be used to achieve non-contact manipulation, for biological cells, the use of high voltage could cause damage to the cell. The two common phenomena are temperature rise due to Joule heating and membrane rupture due to high membrane potential. The imposed transmembrane voltage can be calculated as [46]:

$$|V_{tm}| = \frac{1.5|E|r}{\sqrt{1+\omega\tau^2}} \tag{11}$$

where ω is the frequency, r is the cell radius, $|E|$ is the strength of the electric field, and τ is the time constant given by:

$$\tau = \frac{rC_m(\rho_{cyto} + 1/2\rho_{med})}{1 + rG_m(\rho_{cyto} + 1/2\rho_{med})} \tag{12}$$

where C_m and G_m are the membrane capacitance and the conductance, respectively. ρ_{cyto} is the resistivities of cytoplasm while ρ_{med} is the resistivities of the medium, respectively. Unlike conventional microfluidic devices, the proposed system can easily adjust the height between the microchip and the embryo on the Petri dish. It is necessary to know the suitable operating voltage for a selected channel height to avoid cell lysis. Hence, a study between the height of the microchip to the electric field acting on the embryo was conducted. Table II shows the simulation result of the strength of the electric field under different settings. It can be observed that when the height decreases by every 50 μm, the supply voltage should be decreased by 1 V to maintain the same strength of the electric field acting on the embryo.

TABLE II
Strength of Electric Field With Different Input Voltages and Different Microchip Heights (V/m)

	5V	6V	7V	8V	9V
$100\mu m$	12259	14711	17163	19615	22067
$150\mu m$	11088	13306	15524	17742	19960
$200\mu m$	9747	11697	13646	15596	17546
$250\mu m$	8393	10072	11751	13430	15108

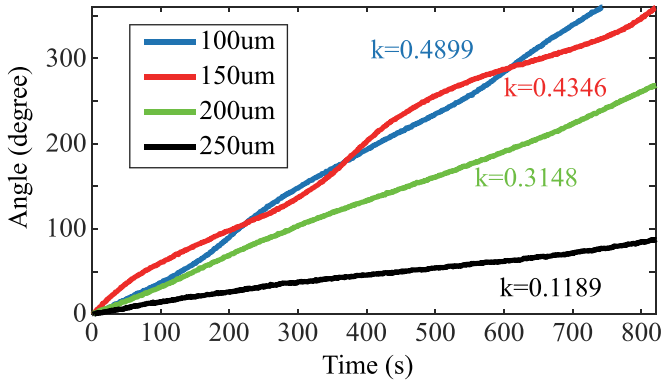

Fig. 9. Rotation angle of embryo versus time with different microchip height circumstance.

TABLE III
Angular Velocity With Different Input Voltages and Different Microchip Heights ($^\circ/s$)

	5V	6V	7V	8V	9V
$100\mu m$	0.4899	0.6754	1.074	1.376	1.849
$150\mu m$	0.4346	0.5825	0.7072	1.114	1.318
$200\mu m$	0.3148	0.3825	0.578	0.7378	0.8532

According to (6), the angular velocity is dependent on the strength of the electric field. To examine the effect of the channel height on the rotation, experiments were conducted to measure the angular position of the embryos over time under different channel heights. The results are plotted in Fig. 9. It can be observed that increasing the height of the channel leads to a decrease in the rotation speed. The speed reduction is approximately equal to the square root of the field strength, which aligns with (6).

A table summarizing the angular velocity with different input voltages and different channel heights is shown in Table III. Similar findings can be observed in this table and in Table II and the increment in the voltage or the height results in a similar change in the field strength, suggesting that a 50 μm height difference would need to change the supply voltage by 1 V to maintain the same performance.

As reported in [47], the voltage leading to the dielectric breakdown of cell membrane is about 1 V. Implemented with a microfluidic device, Park *et al.* [29] show that a 1 V signal is

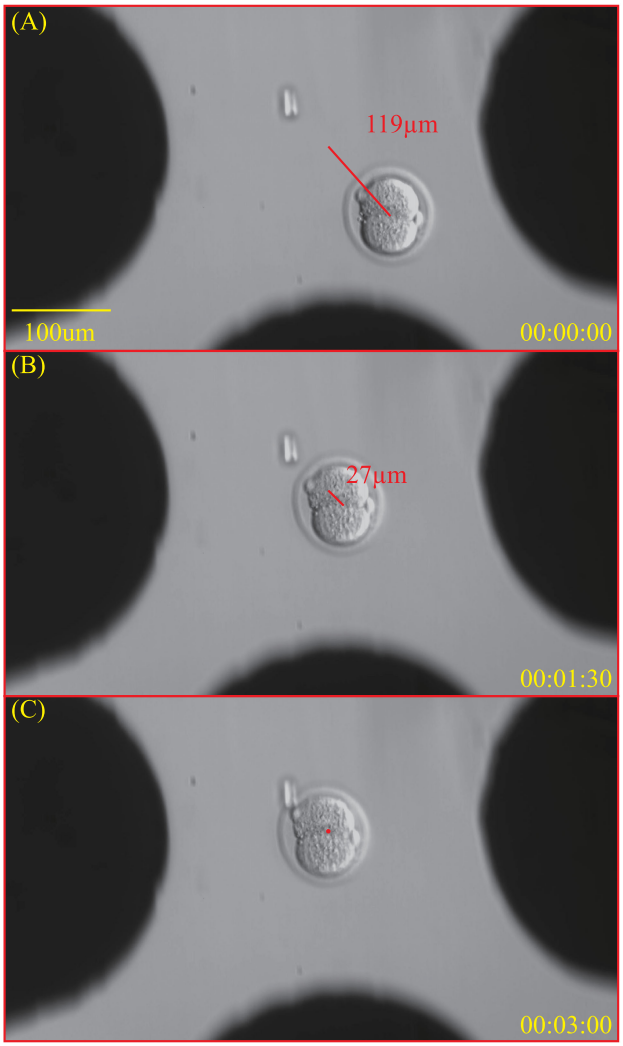

Fig. 10. Embryo is driven to the center of the quadrupole electrodes (A). Embryo in the original place (B). Embryo is rapidly driven by the DEP force (C). The movement becomes slow.

sufficient to rotate an embryo without causing any damage to the embryo. The embryo, with a radius of 50 μm, is in contact with the microchip ($h = r = 50\mu m$). Hence, in this experiment, the microchip was placed 200 μm above the embryo and a maximum voltage of 3 V was used.

B. Embryo Translation By DEP Force

1) Open-Loop Translation: As discussed in Section III, the value of the induced DEP force is the smallest when the embryo is located at the center of the quadrupole electrodes (Fig. 3A). To manipulate an embryo, the embryo needs to be trapped by the DEP-tweezers and the substrate on the stage is moved to provide relative motion. Experimental results on embryo trapping are shown in Fig. 10. Initially, the embryo was located at 119 μm from the center of the electrodes. When the electrodes were powered on, the embryo was driven to the center by the DEP force. The embryo was first displaced by 92 μm at a higher speed (Fig. 10B), and slowed down and displaced to the center of the

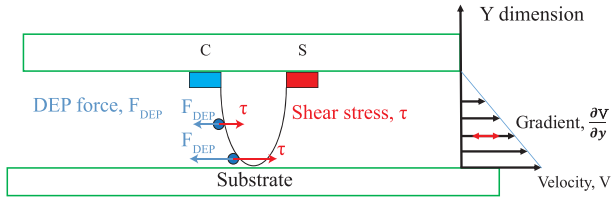

Fig. 11. Force analysis of an embryo in an aqueous environment.

electrodes after 3 seconds (Fig. 10C). The decreasing speed in the embryo shows that the DEP force acting on it is weaker when it approaches the center of the electrodes, which also confirms the result from the simulation shown in Fig. 3A.

After successful trapping, the substrate on the stage starts to transfer to bring the embryo to a new location. During the manipulation, the trapped embryo could still experience a shift in the position, mainly due to the shear stress caused by the fluid. Fig. 11 shows the force analysis of the embryo in the microchannel. When there is a relative motion between the substrate and the microchip, embryos in the microchannel are dragged by the shear stress from the medium. According to the no-slip condition, the velocity of the medium follows a linear velocity profile along with the channel height h, and matches with the velocity at the top (stationary) and bottom (stage velocity, V). For an embryo located near the substrate, shear stress (τ) is induced, acting equally and oppositely on the fluid and the substrate, with a differential relation:

$$\tau = \mu \frac{\partial V}{\partial y} \tag{13}$$

where μ is the viscosity of the medium.

To hold the embryo firmly within the center area, the shear force acting on the embryo must be equal to or less than the nDEP force generated from the microchip ($\tau \leq F_{DEP}$). Therefore, the maximum velocity of the stage must satisfy the equation:

$$M \frac{V_{max}}{h}(2\pi r^2) = 2\pi r^3 \varepsilon_m \cdot Re[K(\omega)] \cdot \bigtriangledown E^2 \tag{14}$$

$$V_{max} = \frac{r\varepsilon_m \cdot Re[K(\omega)] \cdot \bigtriangledown E^2}{M} \cdot h \tag{15}$$

where the velocity at the boundary is $\frac{V}{h}$ and the surface area of a half-spherical object is $2\pi r^2$.

The dynamic shift in the embryo position during the high-speed translation process could lead to a larger DEP force acting on the embryo at the new position, balancing the large drag force induced by the platform according to (14). Although this is advantageous to avoid the embryo from escaping the trap zone, it could increase the possibility of embryo death. To study the relationship between the velocity of the moving stage and the position offset, an experiment was conducted to observe the embryo when the substrate on the stage is moving at different speeds, as shown in Fig. 12A. Based on the results, if the velocity of the stage was 4 μm/s, the position offset of the embryo was approximately 125 px. If the speed was increased to 5 μm/s,

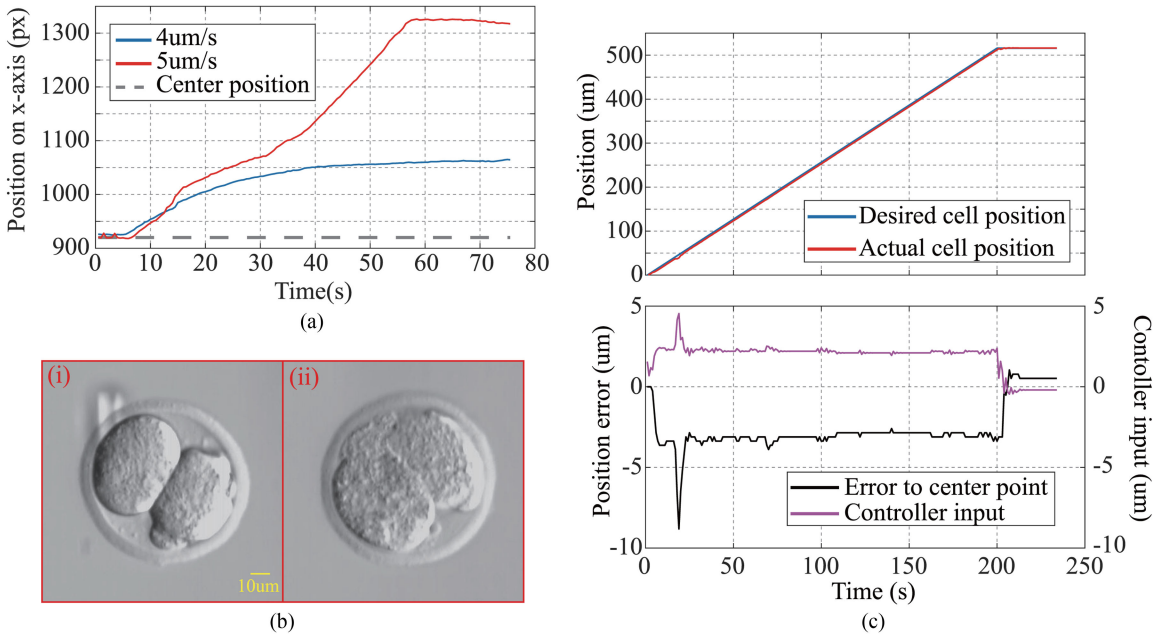

Fig. 12. (a). Embryo hold by DEP and being transferred in different speed (b). i. A complete embryo ii. Embryo broken after transferred at $5\mu m/s$ (c). Path following translation.

the offset position was increased to approximately 400 px. In both cases, the embryo was remained trapped throughout the manipulation process. Nevertheless, it can be observed that the use of a high translation speed of the stage (5 μm/s) can affect the embryo being manipulated. After manipulation, the shape of the blastomere inside the embryo was distorted, as shown in Fig. 12B (i) and (ii). The shape distortion was not observed when the stage velocity was set to 4 μm/s. Hence, the speed was set to 4 μm/s or below, and the maximum position offset of the embryo was set to $x_o = 400px$ in (9a) to minimize the effect on the embryo.

2) Path Following of Embryo Manipulation With PID Control: The trapped embryo was translated to the desired location through the relative movement from the substrate. During this process, uncertainty or instability caused by the irregular fluid flow and surface uniformity may affect the path for embryo translation. Therefore, a PID controller was introduced for precise manipulation. With the presence of multiple embryos, proper path planning is also needed to aid the transport of the trapped embryo to the desired location without colliding with other embryos.

In the experiment, the embryo was set to displace over a distance of 500 μm and the desired path was generated using a velocity of 2.5 μm/s. The parameters used in the PID controller are as follows: the control gains are $K_p = 0.6$, $K_i = 0$, $K_d = 0.001$, and the time constant $T_f = 0.2\,s$. Fig. 12C shows the performance of the PID controller. The embryo can follow closely to the desired path with an average error of within 5 μm throughout the tracking. This error is small compared with the size of an embryo, as well as the translational distance. Fig. 13 shows snapshots of the embryo at different instances during the manipulation.

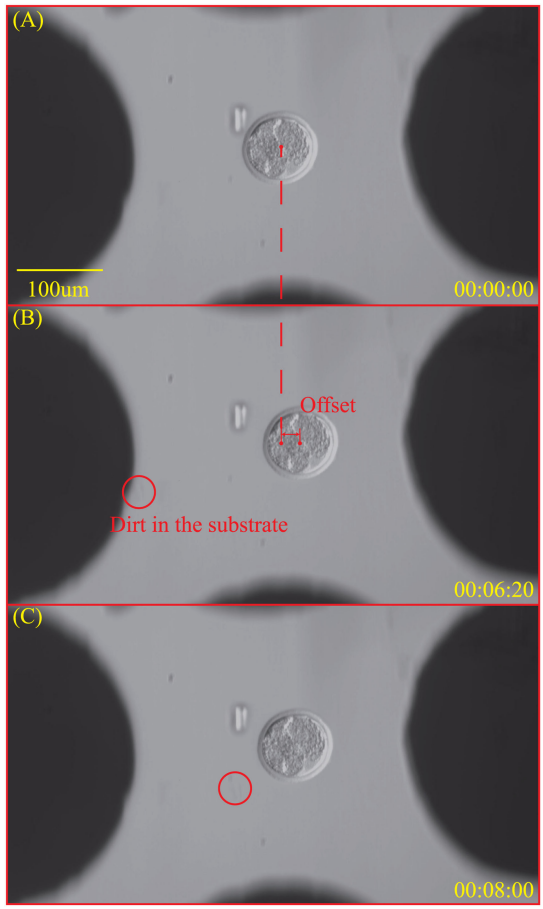

Fig. 13. Embryo translation (A). Embryo in the initial position (B). An offset occurs when the embryo is transferred (C). Embryo is back to the center of the microchip after translation procedure.

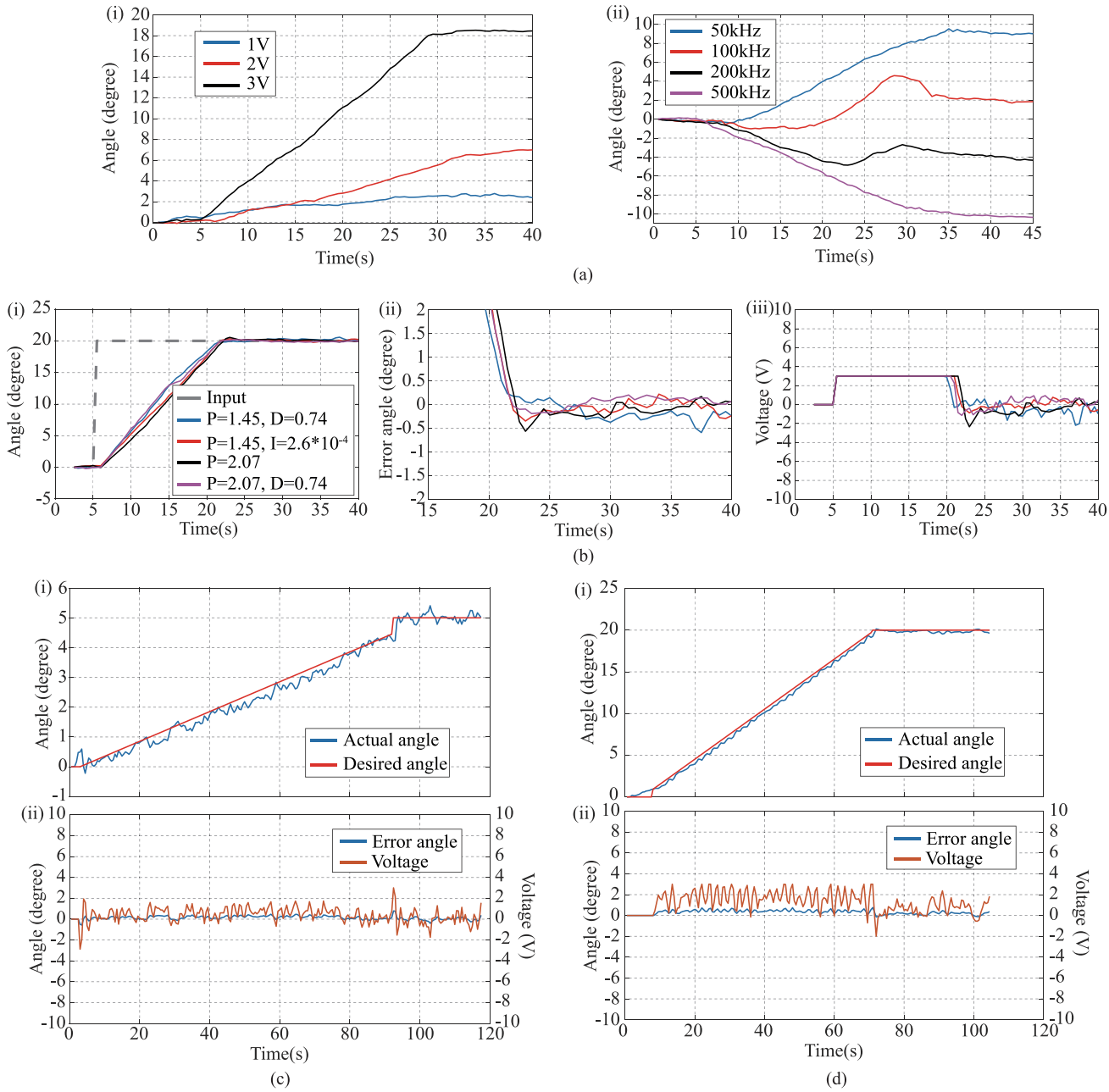

Fig. 14. (a). Embryo open-loop rotation with different inputs i. Different voltage inputs ii. Different frequency inputs (b). Step response embryo rotation with different PID parameters i. Embryo angle versus time ii. Error angle versus time iii. Voltage input versus time (c). Embryo Rotation at $0.05°/s$ (d). Embryo Rotation at $0.29°/s$.

C. Embryo Rotation By ER

1) Open-Loop Rotation: In contrast to embryo translation, the electric field generated through the electrodes is directly used to adjust the orientation of the embryo. As shown in (4), the ER torque is proportional to the square of the electric field, which is primarily related to the voltage amplitude of the signal. The open-loop experiments were conducted by applying different voltage amplitudes to the electrodes (Fig. 14A (i)) and their corresponding angular velocities of the embryo were measured. When the voltage was 3 V, the angular velocity was approximately $0.72°/s$. If the voltage decreased to 1 V, the angular velocity dropped to $0.08°/s$ (Fig. 14A (ii)).

As shown in (4), the sign of the ER torque is dependent on the imaginary part of the CM factor. Through experiments, it can be observed that the crossover frequency for the two-cell embryo is approximately 150 kHz (Fig. 14A (ii)). When the signal frequency was set as at 100 kHz or below, the imaginary part of the CM factor was positive and the embryo rotates in a clockwise direction. In contrast, if the voltage frequency was set to 200 kHz or higher, the rotation direction of the embryo changed from clockwise to counterclockwise.

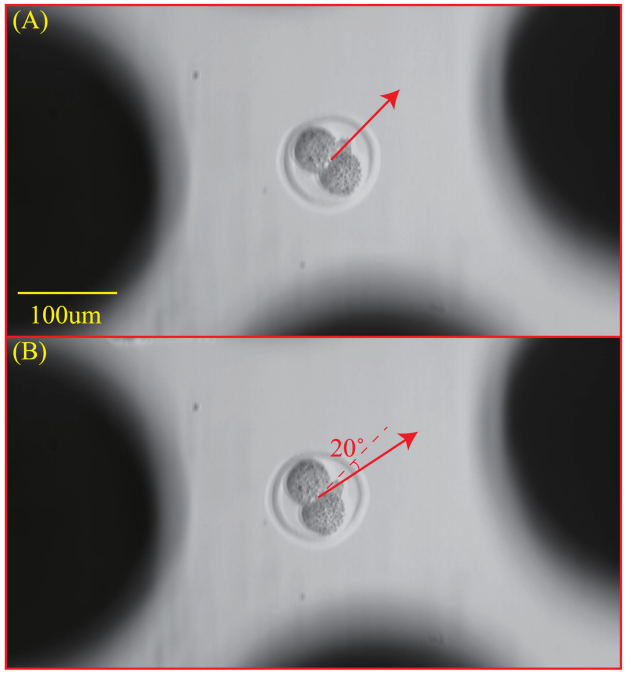

Fig. 15. Image of embryo rotation at $0.29^\circ/s$.

2) Step Response Rotation: Experiments on precise orientation control of the embryo were also conducted. As discussed previously, the maximum applied voltage should be limited to 3 V to avoid possible damage to the embryo. The embryo is required to rotate by an angle given with respect to its original orientation, and a PID controller was employed to track the rotational motion of the embryo. The angle was set to 20° and the experimental results using different parameters are plotted in Fig. 14B. Figs. 14B (i). (ii) and (iii) show the angle, angular error, and input voltage for the controller with different parameter settings, respectively. It can be observed that the embryo was successfully rotated by 20° under different settings. The angular velocity was approximately $1.17^\circ/s$ (Fig. 14B (i)) as the voltage applied to the electrodes was within 3 V. The steady-state angular position error was less than 0.5°. At $k_p = 2.07, k_d = 0.74$, the overshoot and the steady-state error in the process were the smallest compared with the other three configurations. Therefore, the controller setup with $k_p = 2.07, k_d = 0.74$ was selected for embryo rotation.

3) Rotation With the Desired Velocity: The performance of the embryo rotating at a constant velocity to the desired angle is shown in Figs. 14C and 14D. The angular velocity was set to $0.05^\circ/s$ and $0.29^\circ/s$, respectively, and the final angle was 5° and 20° respectively. The actual angle of the embryo over time is shown in Figs. 14C,14D(i), and the angular error and the voltage input are shown in Figs. 14C,14D(ii). For both cases, the embryo was successfully rotated to the desired orientation, but a clear fluctuation was observed. The angular error in Fig. 14C (ii) shows that since the parameters in the PID controller were optimized based on earlier results, the error was minimal. However, the performance was not satisfactory when the angular velocity was set to $0.29^\circ/s$. The voltage data in Fig. 14D (ii) shows that a bias of 1 V in exists the process and Fig. 14D (i) also illustrates that the actual angle cannot follow the desired angle over time because there is a lag between the actual angle and the desired angle. One reason for the lag is due to the limit of maximum voltage input of 3 V and the inappropriate PID configuration with a small K_p value. Figs. 15A and B show how an embryo was rotated by 20°.

VI. Conclusion

Embryo translation and rotation is an important task in the biological field. In this paper, a robotic nDEP-tweezers was developed to enable embryo manipulation with a 3D platform. The system consists of a quadrupole electrode microchip and a micromanipulation system. Image processing techniques were employed to extract the position as well as the orientation of an embryo. A PID controller was adopted to precisely drag and rotate the embryo to the desired location with the required orientation. Experiments confirm that the system can successfully manipulate and rotate embryos with high precision. This system offers a non-contact, low cost, flexible, and effective method for embryo manipulation, avoiding the adhesion force between the embryo and the tool. Compared with the microfluidic device, the open environment of the system provides the flexibility for embryo culture and development after embryo manipulation.

Acknowledgment

The authors gratefully acknowledge assistance from Nadirah Damseh from the Sick Kids Hospital, Toronto, Canada with the biological issues related to this work and the Center of Phenogenomics, Toronto, Canada for providing the embryos.

References

[1] R. M. Schultz and C. J. Williams, "The science of art," *Sci.*, vol. 296, no. 5576, pp. 2188–2190, 2002.
[2] P. Devroey and A. Van Steirteghem, "A review of ten years experience of icsi," *Hum. Reprod. Update*, vol. 10, no. 1, pp. 19–28, 2004.
[3] L. Wolpert, *Principles of Development*, New York, NY, USA: Oxford Univ. Press, 2015.
[4] S. Nilufar, "Automatic blood cell classification based on joint histogram based feature and Bhattacharya kernel," in *Proc. 42nd Asilomar Conf. Signals, Syst. Comput.*, 2008, pp. 1915–1918.
[5] I. A. Ajamieh *et al.*, "Automatic system for the blastocyst embryo manipulation and rotation," *Annal. Biomed. Eng.*, vol. 48, no. 1, pp. 426–436, 2020.
[6] Z. Wang *et al.*, "Visual servoed three-dimensional cell rotation system," *IEEE Trans. Biomed. Eng.*, vol. 62, no. 10, pp. 2498–2507, Oct. 2015.
[7] C. Leung *et al.*, "Three-dimensional rotation of mouse embryos," *IEEE Trans. Biomed. Eng.*, vol. 59, no. 4, pp. 1049–1056, Apr. 2012.
[8] Y. Sun and B. J. Nelson, "Biological cell injection using an autonomous microrobotic system," *Int. J. Robot. Res.*, vol. 21, no. 10-11, pp. 861–868, 2002.
[9] K. Yanagida *et al.*, "The usefulness of a piezo-micromanipulator in intracytoplasmic sperm injection in humans," *Hum. Reprod.*, vol. 14, no. 2, pp. 448–453, 1999.
[10] C. Y. Wong and J. K. Mills, "Automation and optimization of multipulse laser zona drilling of mouse embryos during embryo biopsy," *IEEE Trans. Biomed. Eng.*, vol. 64, no. 3, pp. 629–636, Mar. 2016.
[11] T. Nakayama *et al.*, "A new assisted hatching technique using a piezo-micromanipulator," *Fertil. Steril.*, vol. 69, no. 4, pp. 784–788, 1998.

[12] H. K. Chu *et al.*, "Dual-arm micromanipulation and handling of objects through visual images," in *Proc. IEEE Int. Conf. Mechatron. Autom.*, 2012, pp. 813–818.
[13] J. Liu *et al.*, "Automated vitrification of embryos: A robotics approach," *IEEE Robot. Autom. Mag.*, vol. 22, no. 2, pp. 33–40, Jun. 2015.
[14] Z. Zhang *et al.*, "Robotic pick-and-place of multiple embryos for vitrification," *IEEE Robot. Autom. Lett.*, vol. 2, no. 2, pp. 570–576, 2016.
[15] M. A. Rahman *et al.*, "Cooperative micromanipulation using the independent actuation of fifty microrobots in parallel," *Sci. Rep.*, vol. 7, no. 1, pp. 1–11, 2017.
[16] N. Takahashi *et al.*, "Analysis of geometric and motion characteristics of bubble microrobots for caging based cell manipulation," in *Proc. IEEE Int. Conf. Nano/Molecular Med. Eng*, 2016.
[17] K. Ino *et al.*, "Cell patterning using magnetite nanoparticles and magnetic force," *Biotechnol. Bioeng.*, vol. 97, no. 5, pp. 1309–1317, 2007.
[18] J. El Ali *et al.*, "Cells on chips," *Nature*, vol. 442, no. 7101, p. 403, 2006.
[19] J. K. Valley *et al.*, "Optoelectronic tweezers as a tool for parallel single-cell manipulation and stimulation," *IEEE Trans. Biomed. Circuit. Syst.*, vol. 3, no. 6, pp. 424–431, Dec. 2009.
[20] T. Yasukawa *et al.*, "Electrophoretic cell manipulation and electrochemical gene-function analysis based on a yeast two-hybrid system in a microfluidic device," *Anal. Chem.*, vol. 80, no. 10, pp. 3722–3727, 2008.
[21] Z. Huan *et al.*, "Characterization of a honeycomb-like scaffold with dielectrophoresis-based patterning for tissue engineering," *IEEE Trans. Biomed. Eng.*, vol. 64, no. 4, pp. 755–764, Apr. 2017.
[22] Y. Eguchi *et al.*, "Control of orientation of rat schwann cells using an 8-t static magnetic field," *Neurosci. Lett.*, vol. 351, no. 2, pp. 130–132, 2003.
[23] D. J. Collins *et al.*, "Two-dimensional single-cell patterning with one cell per well driven by surface acoustic waves," *Nat. Commun.*, vol. 6, p. 8686, 2015.
[24] X. Li *et al.*, "Dynamic trapping and manipulation of biological cells with optical tweezers," *Autom.*, vol. 49, no. 6, pp. 1614–1625, 2013.
[25] S. Bayoudh *et al.*, "Orientation of biological cells using plane-polarized Gaussian beam optical tweezers," *J. Modern Opt.*, vol. 50, no. 10, pp. 1581–1590, 2003.
[26] M. Xie *et al.*, "Automated translational and rotational control of biological cells with a robot-aided optical tweezers manipulation system," *IEEE Trans. Autom. Sci. Eng.*, vol. 13, no. 2, pp. 543–551, Apr. 2015.
[27] Y. Yang *et al.*, "Self-locking optoelectronic tweezers for single-cell and microparticle manipulation across a large area in high conductivity media," *Sci. Rep.*, vol. 6, p. 22630, 2016.
[28] C. Jiang and J. K. Mills, "Planar cell orientation control system using a rotating electric field," *IEEE/ASME Trans. Mechatron.*, vol. 20, no. 5, pp. 2350–2358, Oct. 2015.
[29] J. Park *et al.*, "Design and fabrication of an integrated cell processor for single embryo cell manipulation," *Lab Chip*, vol. 5, no. 1, pp. 91–96, 2005.
[30] I. K. Glasgow *et al.*, "Handling individual mammalian embryos using microfluidics," *IEEE Trans. Biomed. Eng.*, vol. 48, no. 5, pp. 570–578, May 2001.
[31] W. Choi *et al.*, "Dielectrophoretic oocyte selection chip for in vitro fertilization," *Biomed. Microdevices*, vol. 10, no. 3, pp. 337–345, 2008.
[32] J. K. Valley *et al.*, "Preimplantation mouse embryo selection guided by light-induced dielectrophoresis," *PLoS One*, vol. 5, no. 4, p. e10160, 2010.
[33] S. Raty *et al.*, "Embryonic development in the mouse is enhanced via microchannel culture," *Lab Chip*, vol. 4, no. 3, pp. 186–190, 2004.
[34] K. Huang *et al.*, "Automated cell patterning system with a microchip using dielectrophoresis," in *Proc. Int. Conf. Robot. Autom.*, 2019, pp. 634–639.
[35] K. Huang *et al.*, "Microchip system for patterning cells on different substrates via negative dielectrophoresis," *IEEE Trans. Biomed. Circuit. Syst.*, vol. 13, no. 5, pp. 1063–1074, 2019.
[36] W. M. Arnold *et al.*, "Electro-rotation of mouse oocytes: Single-cell measurements of zona-intact and zona-free cells and of the isolated zona pellucida," *Biochimica et Biophysica Acta (BBA)-Biomembranes*, vol. 905, no. 2, pp. 454–464, 1987.
[37] H. A. Pohl, *Dielectrophoresis: The Behavior Neutral Matter Nonuniform Electric Fields (Cambridge Monographs physics)*. Cambridge, U.K.: Cambridge Univ. Press, 1978.
[38] T. B. Jones, "Basic theory of dielectrophoresis and electrorotation," *IEEE Eng. Med. Biol. Mag.*, vol. 22, no. 6, pp. 33–42, Dec. 2003.
[39] H. Fricke, "The electric conductivity and capacity of disperse systems," *Physics*, vol. 1, no. 2, pp. 106–115, 1931.
[40] A. Irimajiri *et al.*, "A dielectric theory of "multi-stratified shell" model with its application to a lymphoma cell," *J. Theor. Biol.*, vol. 78, no. 2, pp. 251–269, 1979.
[41] Y. Huang *et al.*, "Differences in the ac electrodynamics of viable and non-viable yeast cells determined through combined dielectrophoresis and electrorotation studies," *Phy. Med. Biol.*, vol. 37, no. 7, p. 1499, 1992.
[42] P. H. Torr and A. Zisserman, "MLESAC: A new robust estimator with application to estimating image geometry," *Comput. Vis. Image Understanding*, vol. 78, no. 1, pp. 138–156, 2000.
[43] G. L. Kovács *et al.*, "Non-invasive assessment of viability in human embryos fertilized in vitro," *EJIFCC*, vol. 27, no. 2, p. 112, 2016.
[44] V. Noto *et al.*, "Fluorescein diacetate assessment of embryo viability after ultrarapid freezing of human multipronucleate embryos," *Fertility and sterility*, vol. 55, no. 6, pp. 1171–1175, 1991.
[45] S. Hu and D. Sun, "Automatic transportation of biological cells with a robot-tweezer manipulation system," *Int. J. Robot. Res.*, vol. 30, no. 14, pp. 1681–1694, 2011.
[46] H. Schwan, "Dielectrophoresis and rotation of cells," in *Electroporation and Electrofusion in Cell Biology*, Boston, MA: Springer, 1989, pp. 3–21.
[47] U. Zimmermann and G. A. Neil, *Electromanipulation of Cells*, Boca Raton, FL, USA: CRC press, 1996.